Draft version February 2, 2008
Preprint typeset using LaTeX style emulateapj v. 25/04/01

ON THE ROLE OF MAGNETIC FIELDS IN ABUNDANCE DETERMINATIONS

J.M. Borrero
High Altitude Observatory (NCAR), 3080 Center Green Dr. CG-1, Boulder, CO 80301, USA
borrero@ucar.edu

Draft version February 2, 2008

ABSTRACT

Although there is considerable evidence supporting an ubiquitous magnetic field in solar/stellar photospheres, its impact in the determination of abundances has never been quantified. In this work we investigate whether the magnetic field plays a measurable role for this kind of studies. To that end, we carry out simulations of spectral line formation in the presence of a magnetic field, and then use those profiles to derive the abundance of several atomic species (Fe, Si, C and O) neglecting the magnetic field. In this way, we find that the derived iron abundance can be significantly biased, with systematic errors up to 0.1 dex. In the case of silicon, carbon and oxygen their role is very marginal (errors smaller than 0.02 dex). We also find that the effect of the magnetic field strongly depends on its inclination with respect to the observer. We show that fields that are aligned with the observer lead to an underestimation of the real abundance, whereas more inclined ones overestimate it. In the case of a mixture of fields with different inclinations these effects are likely to partly cancel each other out, making the role of the magnetic field even less important. Finally, we derive a simple model that can be used to determine the suitability of a spectral line when we wish to avoid the bias introduced by the neglect of the magnetic field.

Subject headings: Sun: magnetic fields, abundances – Stars: magnetic fields, abundances

1. INTRODUCTION

From the very first determinations of solar and stellar abundances using 1D semi-empirical atmospheric models (e.g. Lambert 1968, Lambert & Warner, B. 1968, Grevesse 1968, Garz et al. 1969) to more recent values obtained from state-of-the-art 3D hydrodynamical simulations (e.g. Asplund et al. 2005a), the role of the magnetic field has rarely been considered. This would be strictly valid only if atomic transitions with zero Landé factors are used in the analysis. Unfortunately this has never been the case. The reason for this is that there are few magnetic insensitive spectral lines having accurate oscillator strengths. In the case of the Sun, the role of the magnetic field has been avoided by arguing that the FTS-disk center spectral atlas (Brault & Neckel 1987; Neckel 1999), which is the most common source to compare observed and simulated line profiles, was recorded around a quiet Sun region.

The existence of significant magnetic flux in quiet Sun regions has passed unnoticed because this magnetic field organizes in patches of opposite polarity[1] over very small scales, leading to a cancellation of the polarization signals. However, there is now strong evidence supporting the omnipresence of magnetic fields in regions previously thought to be void of them (Trujillo Bueno et al. 2004; Manso Sainz et al. 2004). The details about its actual strength and distribution are subject to debate, however.

This is even more critical when disk integrated data is used in stellar abundances studies (e.g. Allende Prieto et al. 2002), in particular if the star is magnetically active (Ap-Bp types), as regions of strong magnetic field (i.e.: starspots) can have a large influence.

Although the magnetic field will mainly affect the polarization signals, it also has an impact on the intensity profiles (Stokes I), being this particularly important because this effect on the intensity profiles adds up regardless of its polarity. If not accounted for, this might lead to systematic errors in the abundance values derived from the fitting. The goal of this work is to asses the importance of neglecting the role of magnetic fields. To that end we will perform simplistic simulations of intensity profiles of various important atomic elements in the presence of a magnetic field. In Section 2 we describe the synthesis code employed, the spectral lines used and we briefly review the Zeemann effect applied to Stokes I. In Section 3 we study how the strength and inclination of the magnetic field taintes the inferred abundances of iron, silicon carbon and oxygen when the existence of this field is neglected. In Section 4 we derive a simple model that is able to quantitatively predict the commited error. Section 5 is devoted to studying if results from our simple modeling could differ significantly if the same investigation is performed using more realistic 3D MHD models. Section 6 summarizes our findings and anticipates possible future work.

2. SPECTRAL LINES SYNTHESIS

2.1. *Synthesis code*

We have employed the SIR code (Ruiz Cobo & del Toro Iniesta 1992) to produce synthetic spectral lines. This code solves the radiative transfer equation in the presence of a magnetized plasma. Although SIR synthesizes the full Stokes vector, we will restrict ourselves to consider only the total intensity, Stokes I, as done in most abundance studies. In addition, SIR allows for the magnetic field vector to be a function of the optical depth, but in this work we will consider it constant.

The Harvard-Smithsonian Reference Atmosphere

[1] In spectropolarimetry, the term positive polarity refers to magnetic fields pointing towards the observer: inclination angles $\gamma < 90^\circ$, while negative polarities refer to magnetic fields pointing away from the observer: $\gamma > 90^\circ$

(HSRA; Gingerich et al. 1971) was used in our calculations. Note that using this 1D LTE semi-empirical model means that we study the impact of the magnetic field alone, that is, we assume that other important ingredients of the spectral line formation are already being accounted for. For instance, the magnetic field couples with the energy and momentum equation, resulting in a modification of the temperature stratification. In our analysis we are assuming that the correct temperature stratification and convective velocity fields are known (i.e.: obtained through realistic 3D simulations) and therefore we focus on the magnetic field. If this was not the case, small errors in the temperature or velocities would dominate over the neglect of the magnetic field.

To account for the convective broadening of the spectral lines we use, unless otherwise specified, a macroturbulent velocity of 2 km s^{-1} and a microturbulent velocity of 1 km s^{-1}. We anticipate (see Section 5) that these values have no particular consequences in our discussion.

2.2. *Spectral line selection*

We have decided to focus our study on four important atomic elements: Fe I, Si I, C I and O I. Iron is particularly important because it shows a large number of atomic transitions at visible wavelengths, and therefore it is often used to investigate solar and stellar atmospheres. In addition, it is commonly used to distinguish whether a star is first or second generation since heavier elements are only produced in Supernova explosions (Christlieb et al. 2002). Silicon is important in the solar context as it is used, together with iron, to compare with meteoritic abundances (Asplund 2000). Oxygen and carbon's importance comes from being the third and fourth most abundant elements in the Universe, respectively. In addition, they have both been targeted as being responsible for the lowering of the solar metallicity (Asplund et al. 2005a), that has caused major discrepancies between helioseismic inversions and solar models (Castro et al. 2007). Therefore, it is worthwhile investigating whether magnetic fields could have something to say in this regard.

In total we consider 57 spectral lines: 29 of Fe I, 15 of Si I, 9 of C I and 4 of O I. Their properties are summarized in Table 1. They have been adopted from Asplund (2000) and Asplund et al. (2000, 2004, 2005b). We have rejected those lines for which accurate collisional parameters (under the ABO theory; Anstee & O'Mara 1995; Barklem & O'Mara 1997; Barklem et al. 1998) were not found. Note that only one line, Si I 5665.555 Å has a zero Landé factor: $g_{\rm eff} = 0$. Several neutral iron and carbon lines are potentially very sensitive to magnetic fields: $g_{\rm eff} \gtrapprox 2$.

2.3. *Intensity profiles under the presence of a magnetic field*

Ignoring off-diagonal elements in the propagation matrix, the main contributor to the intensity profiles is η_I (Wittmann 1974; del Toro Iniesta 2003):

$$\eta_I = 1 + \frac{\eta_0}{2}\left\{\phi_p \sin^2\gamma + \frac{1}{2}[\phi_b + \phi_r](1+\cos^2\gamma)\right\} \quad (1)$$

where η_0 is related to the abundance of the element, the excitation potential of the lower level and the transition probability of the atomic transition (Landi Degl'Innocenti 1976). γ refers to the inclination of the magnetic field vector with respect to the observer. Since it appears as $\cos^2\gamma$ and $\sin^2\gamma$, its contribution is the same regardless of the polarity of the magnetic field (see Footnote 1). Treating the real Zeemann pattern as an effective triplet ($J = 1 \rightarrow J = 0$), the functions ϕ_p, ϕ_r and ϕ_b refer to the Voigt profiles for the Π ($\Delta M = 0$), blue ($\Delta M = -1$) and red ($\Delta M = 1$) components of the Zeeman pattern, respectively. The former is centered at λ_0 (central laboratory wavelength), whereas the latter ones are shifted by an amount $\pm\lambda_B$ with respect to the Π component.

$$\lambda_B = \mathcal{C} g_{\rm eff} B \lambda_0^2 \quad (2)$$

where $C = 4.67 \times 10^{-13}$ [Å Gauss]$^{-1}$, B is the strength of the magnetic field (measured in Gauss), and $g_{\rm eff}$ is the effective Landé factor of the spectral line.

A number of remarks are in order. First of all, in the absence of a magnetic field (or if $g_{\rm eff} = 0$), $\phi_p = \phi_r = \phi_b$ and therefore $\eta_I = 1 + \eta_0\phi_p/2$. Also, it is interesting to see that the blue and red components are always present independently of the orientation of the field. When the field is small enough the splitting is much smaller that the Doppler width of the spectral line, $\lambda_B \ll \Delta\lambda_{\rm D}$, causing the spectral line to broaden. In the opposite case, $\lambda_B \gg \Delta\lambda_{\rm D}$, they appear as two separate spectral lines with half the strength of the spectral line in the absence of magnetic field. Finally, the central Π component vanishes for magnetic fields aligned with the observer ($\gamma = 0$) causing the line core to desaturate.

3. EFFECTS ON THE MAGNETIC FIELD IN THE ABUNDANCE OF FE, SI, C AND O

We now proceed to calculate synthetic Stokes I profiles of the spectral lines in Table 1. We use the numerical code and the atmospheric model described in Sect 2.1. We consider a magnetic field with a varying strength and inclination: $B = [0, 500]$ Gauss, $\gamma = [0, 90]$ deg. We consider also standard solar abundances: $\log\epsilon_{Fe} = 7.45$ (Asplund et al. 2000), $\log\epsilon_{Si} = 7.51$ (Asplund 2000), $\log\epsilon_C = 8.39$ (Asplund et al. 2005b) and $\log\epsilon_O = 8.66$ (Asplund et al. 2004). The resulting profiles are then fitted with different abundances but assuming that there is no magnetic field. For Fe I we use $\log\epsilon_{Fe} = [7.30, 7.80]$ in steps of 0.01. For Si I and O I we consider $\log\epsilon_{Si} = [7.48, 7.54]$ and $\log\epsilon_O = [8.62, 8.70]$, respectively, both in steps of 0.002. Finally, for C I we use $\log\epsilon_C = [8.32, 8.46]$ in steps of 0.005.

From the comparison of the original profiles with magnetic field and fixed abundance with those where the abundance varies and the magnetic field is neglected, we obtain a $\chi^2 - \log\epsilon$ curve for each spectral line. We therefore infer for each line an optimum abundance, as the one that minimizes the χ^2 curve. No other free parameters are considered. An example of this process is presented in Figure 1 using the spectral line Fe I 6136.994 Å a magnetic field of $B = 250$ Gauss and $\gamma = 60°$. The final inferred abundance is obtained as the mean of the best-fit abundances from all spectral lines of that atomic element.

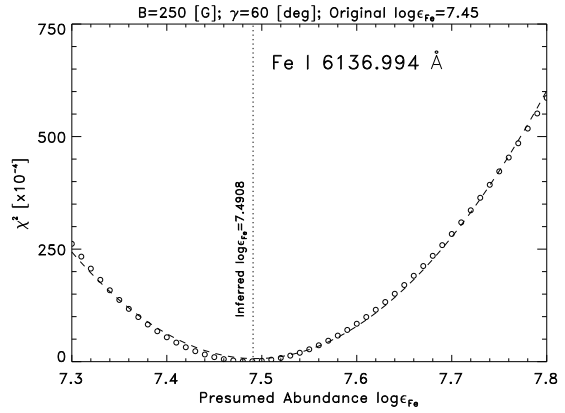

FIG. 1.— χ^2 between the intensity profile of Fe I 6136.994 Å with magnetic field ($B = 250$ Gauss; $\gamma = 60°$) and an iron abundance of $\log \epsilon_{Fe} = 7.45$, and the intensity profile of the same spectral line without magnetic field, as a function of the abundance. The abundance that produces the best fit to the former profile is $\log \epsilon_{Fe} \simeq 7.49$.

Figure 2 presents the errors $\Delta \log \epsilon = \log \epsilon_{\rm fit} - \log \epsilon_{\rm real}$ (as a function of the magnetic field strength and inclination) introduced in the abundance of Fe I, Si I, C I and O I, when the magnetic field is not accounted for. As expected, the larger the field strength the larger the error. Neutral iron, with up to $\Delta \log \epsilon_{\rm Fe} \leq 0.1$, presents the largest deviations. For the rest of considered elements the magnetic field seems to have only a marginal effect: $\Delta \log \epsilon_{\rm Si} \leq 0.01$ and $\Delta \log \epsilon_{\rm C,O} \leq 0.02$.

We also find that vertical fields underestimate the correct abundance, whereas the opposite happens for more inclined magnetic fields. This can be explained attending to Sect 2.3 (Equation 1). For vertical magnetic fields, $\gamma = 0°$, the Π component of the Zeemann pattern is absent, leading to a desaturation of the core intensity and therefore requiring a smaller abundance to fit the line profile. An example with Fe I 5250.209 Å is presented in Figure 3 (left panel). However, when the magnetic field is horizontal, $\gamma = 90°$, the line mainly broadens and thus yieling a larger abundance. See example for Fe I 6200.313 Å in Figure 3 (right panel).

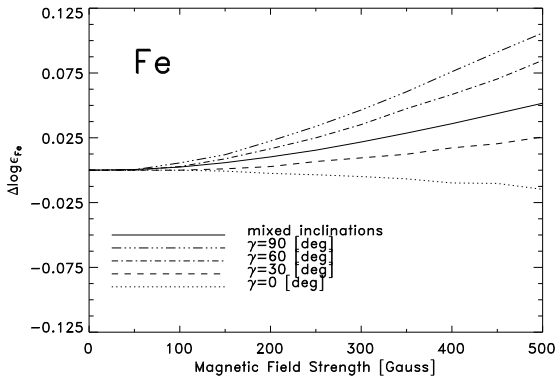

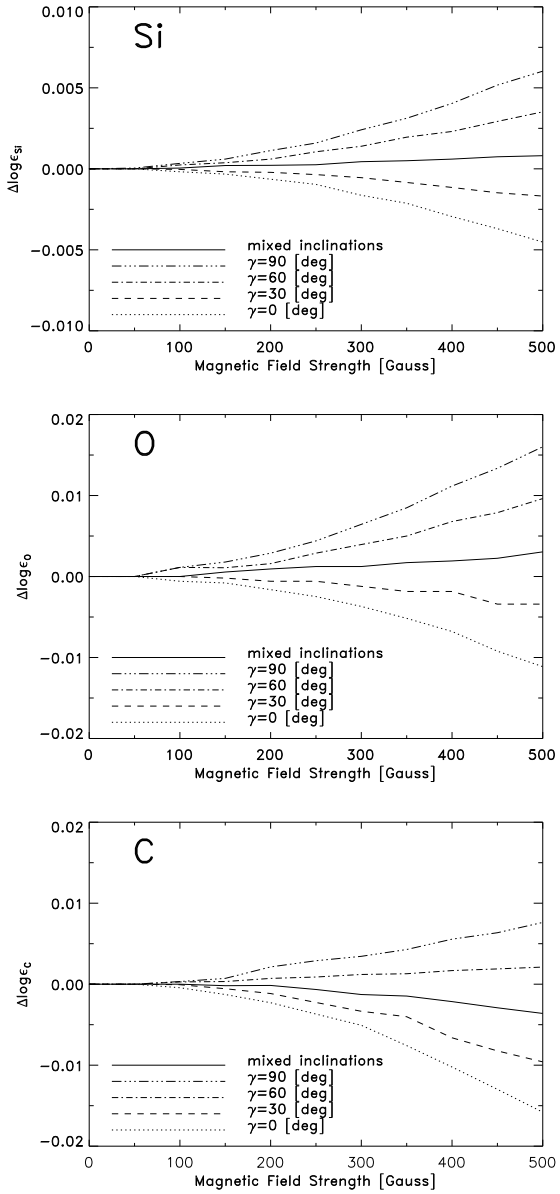

FIG. 2.— Errors in the inferred abundances $\Delta \log \epsilon = \log \epsilon_{\rm fit} - \log \epsilon_{\rm real}$ when the role of the magnetic field is neglected, as a function of the magnetic field strength for 4 different inclinations: $\gamma = 0°$ (dotted line; vertical magnetic field), $\gamma = 30°$ (dashed), $\gamma = 60°$ (dashed-dotted) and $\gamma = 90°$ (dashed-triple dotted; horizontal magnetic field). Solid lines indicate a mixture of field inclinations, in which profiles obtained with the previous 4 inclinations are averaged before inferring an abundance.

We must also consider that different regions of solar and stellar atmospheres can posses magnetic fields with different inclinations. For instance, in the case of the solar granulation, where the field is mostly horizontal in the granules (upflowing gas), but is generally vertical in intergranular lanes (downflowing gas). Since the inclination that matters is with respect to the observer, this situation reverses as we move towards higher latitudes or towards the solar limb. Many other low and intermediate-mass stars also posses an outer convective layer. In addition, strong magnetic concentrations also display a variety of inclinations: star-sunspots (umbra and penumbra), pores, network regions etc. Although they are normally avoided in the Sun, in the stellar case they certainly contribute to the observed

profiles.

Since vertical and horizontal fields seems to have opposite effects in the derived abundance it is appropriate to study whether they can cancel each other out when a mixture of different inclinations is present. To study this effect we have carried out a similar experiment as the ones previously presented, being now the difference that we average the intensity profiles obtained with 4 different inclinations, $\gamma = 0, 30, 60, 90^\circ$ (with the same field strength) before inferring an abundance for each spectral line. In this case, the errors in the retrieved abundance are much smaller (see solid line in Figure 2), being only perceptible for the case of neutral iron: $\Delta \log \epsilon_{\rm Fe} \leq 0.02$. This simulation is very simple in the sense that it does not include different temperature stratifications, different velocity fields, etc. However, it helps to highlight that the aforementioned cancellation effect can indeed take place. This cancellation effect in Stokes I due to vertical and horinzontal magnetic fields, is similar in a way to the cancellation of circular polarization signals due to a mixture of magnetic fields pointing towards and away from the observer.

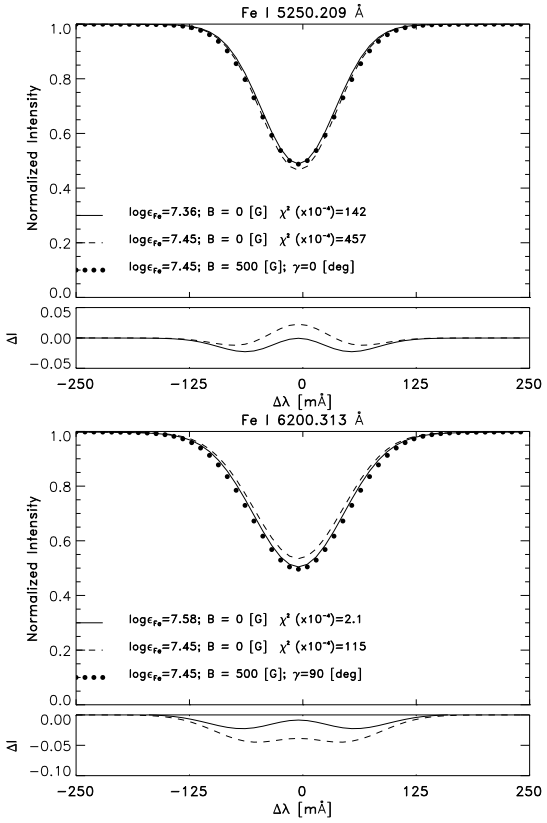

FIG. 3.— Filled circles are intensity profiles obtained with the nominal iron abundance of $\log \epsilon_{Fe} = 7.45$, a magnetic field strength of $B = 500$ Gauss and inclinations of $\gamma = 0^\circ$ (left panel) and $\gamma = 90^\circ$ (right panel). Those profiles are then fitted without a magnetic field. When the original profile is affected by a vertical magnetic field, the best fit (solid lines) is obtained by underestimating the original abundance. The opposite occurs for horizontal magnetic fields.

From these results we conclude that the effect of neglecting the role of the magnetic field in abundance determinations strongly depends on the atomic specie and spectral line under consideration, as well as the strength and inclination of the magnetic field. From the four atomic species considered, it appears to have a measurable effect in the case of Fe I only. It could be marginally important for Si I, C I and O I only if the magnetic field had a clearly preferred orientation. In stellar atmospheres, where we observe disk-integrated signals, this is unlikely the case. In addition, magnetic fields do not appear as a plausible source of error in the current controversy of the solar carbon and oxygen abundance.

4. A PHENOMENOLOGICAL MODEL

The different behavior seen in Fe I as compared to the other three elements considered cannot be understood in terms of the magnetic sensitivity of the lines used, as most of them have similar Landé factors ranging from $g_{\rm eff} = 1 - 2$. The source of these differences must be therefore thermodynamic. In this section we will develop a tool to differentiate whether a given spectral line of a particular atomic element is prone to yield unreliable abundances. To that end we assume that the error in the inferred abundances, that appears as a consequence of neglecting the magnetic field, is directly proportional to the changes in the line profile in the presence of a magnetic field:

$$\Delta \log \epsilon \propto \max \left\| \frac{\partial I}{\partial B} \right\| \tag{3}$$

where we use maximum of the absolute value since the derivative changes sign as a function of wavelength. Attending Equation 1, we will model the intensity profile as a combination of three Gaussian, where two of them are shifted by an amount $\pm\lambda_B$ with respect to the central laboratory wavelength λ_0. The third Gaussian is centered at λ_0 and possesses twice the strength of the other two.

$$I(\lambda) = 1 - \frac{[1-I_0]\sin^2\gamma}{2} e^{-\frac{(\lambda-\lambda_0)^2}{\Delta\lambda^2}} - \frac{[1-I_0](\cos^2\gamma+1)}{4}\left\{ e^{-\frac{(\lambda-\lambda_0-\lambda_B)^2}{\Delta\lambda^2}} + e^{-\frac{(\lambda-\lambda_0+\lambda_B)^2}{\Delta\lambda^2}} \right\} \tag{4}$$

where I_0 and $\Delta\lambda$ refer to the core intensity and the Doppler width of the spectral line in the absence of magnetic field. That is,

$$\lim_{B\rightarrow 0} I(\lambda) = 1 - (1-I_0) e^{-\frac{(\lambda-\lambda_0)^2}{\Delta\lambda^2}} \tag{5}$$

Note that $\Delta\lambda$ is related to the HWHM of the Gaussian profile by a constant factor: HWHM$=\sqrt{\log 2}\Delta\lambda \simeq 0.832\Delta\lambda$. Table 1 presents the values of I_0 and $\Delta\lambda$ obtained from a Gaussian fit to the intensity profiles in the absence of magnetic field for each spectral line. Finally, Equations (2)-(4) can be combined to write:

$$\Delta \log \epsilon \propto \max \left\| \frac{1-I_0}{2\Delta\lambda^2}(\cos^2\gamma+1)\mathcal{C} g_{\rm eff}\lambda_0^2 [(\lambda-\lambda_0+ +\lambda_B) e^{-\frac{(\lambda-\lambda_0+\lambda_B)^2}{\Delta\lambda^2}} - (\lambda-\lambda_0-\lambda_B) e^{-\frac{(\lambda-\lambda_0-\lambda_B)^2}{\Delta\lambda^2}}] \right\| \tag{6}$$

This procedure is very similar to the one used in Cabrera Solana et al. (2005) but using Stokes I instead of the circular polarization, Stokes V. Equation 6 allows to predict the effect of ignoring the magnetic field using: properties of the spectral line (regardless of the atomic specie) in the

absence of a magnetic field (I_0, $\Delta\lambda$, λ_0), Landé factor $g_{\rm eff}$ (given by the electronic configurations) and the strength of the magnetic field (used to calculate λ_B). Note that the inclination of the magnetic field does not play any role. The factor $[\cos^2\gamma+1]$ does not help to explain the fact that for vertical fields $\Delta\log\epsilon < 0$, but $\Delta\log\epsilon > 0$ for horizontal fields. Therefore it is more appropriate to write:

$$\Delta\log\epsilon = \mathcal{A}(\gamma)\max\left\|\frac{1-I_0}{2\Delta\lambda^2}\mathcal{C}g_{\rm eff}\lambda_0^2[(\lambda-\lambda_0+ \right.$$
$$\left. +\lambda_B)e^{-\frac{(\lambda-\lambda_0+\lambda_B)^2}{\Delta\lambda^2}} - (\lambda-\lambda_0-\lambda_B)e^{-\frac{(\lambda-\lambda_0-\lambda_B)^2}{\Delta\lambda^2}}]\right\| \quad (7)$$

where the calibration constant $\mathcal{A}(\gamma)$ can be determined for different field inclinations using our results in Section 3. This is done in Figure 4, where we plot the left-hand side term of Equation 6 (obtained from Section 3) versus the right hand-side of the same equation (evaluated using Table 1) for two limiting inclinations: $\gamma = 0°$ (upper panel) and $\gamma = 90°$ (lower panel) for all spectral lines. As it can be seen the correlation is good enough to empirically justify, in first approximation, our assumption in Equation 3. That is, the more a spectral line is affected by the magnetic field, the more unreliable the derived abundance will be if the magnetic field is not considered. In addition, all spectral lines seem to follow a linear relation regardless of the atomic specie. The present model explains why Fe I is affected by the magnetic field more than Si I, C I and O I. As already mentioned, this is not due to the different Landé factors, but rather due to their different sensitivity to thermodynamic parameters: I_0 and $\Delta\lambda$. Narrower and deeper spectral lines ($\Delta\lambda$ and I_0 small) such as the ones from Fe I, are more sensitive to the magnetic field than weak and broad spectral lines.

It is also interesting to notice that the selected C I lines are broader and weaker than those of Si I and O I. Despite this, carbon is affected by the magnetic field as much as the other two (see Fig. 2). The reason is that the employed C I lines are located at larger wavelengths, $\lambda_0^C > \lambda_0^{Si,O}$, and therefore the Zeeman splitting is larger (Eq. 2 and 7).

Since we use the same temperature stratification, the different I_0's and $\Delta\lambda$'s among the selected spectral lines can only be due to differences in the excitation potential of the lower level χ_l, transition probability $\log gf$, and collisional broadening parameters α and σ. In first approximation, the former two would be related to I_0 whereas the latter two determine $\Delta\lambda$.

The utility of the procedure described here lies in the fact that whenever another spectral line is considered (regardless of the atomic element), we can use this method to evaluate Equation 7, and therefore calculate its approximate position in Figure 4. This will give us an idea of the error introduced by ignoring the effects of the magnetic field, even if a numerical code that solves the radiative transfer equation in the presence of a magnetic field is not available.

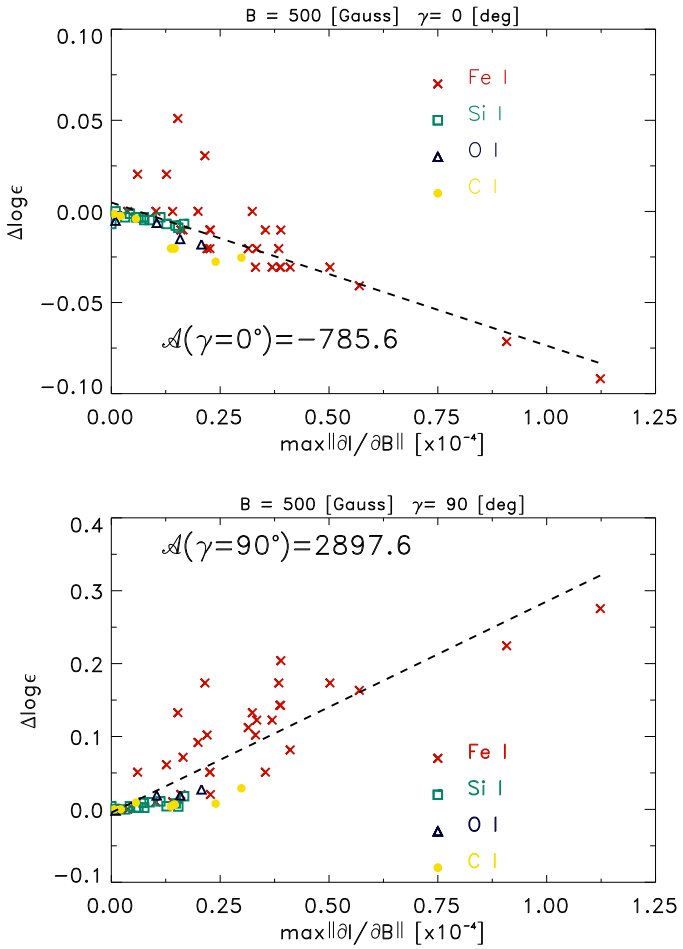

FIG. 4.— Error in the determination of element abundances when using individual spectral lines versus the derivative of its intensity profile with respect to the magnetic field. Red crosses show the 29 Fe I lines from Table 1. Green squares indicate Si I. O I is denoted by blue triangles. Yellow circles show C I lines. A linear fit to the data points is indicated by the black dashed line. The slope of the fitted line is indicated by $\mathcal{A}(\gamma)$. *Top panel*: vertical magnetic field. *Bottom panel*: horizontal magnetic field.

5. CONVECTIVE VS MAGNETIC BROADENING

In our simple 1D model the convective broadening is introduced through the macro and microturbulent velocities, whereas in a more realistic 3D modeling this broadening naturally occurs when adding the profiles emerging from different regions (i.e.: granules and intergranules) in the solar atmosphere. At first glance it seems plausible for this convective broadening to mask the magnetic one, thus making the contribution of the magnetic fields even more negligible. However, we must take into account that the individual intensity profiles emerging from different regions of the solar atmospheres are already affected by the magnetic field. Therefore, when all intensity profiles are added up to produce the corresponding convective broadening, the fingerprints of magnetic field will still be visible.

To prove this statement we have carried out a simple simulation of the process previously described. To that end we synthesize intensity profiles of Fe I 5247.05 Å ($g_{\rm eff}$=2) without magnetic field and no net line-of-sight velocity, but using a macroturbulent velocity of 2 km s^{-1}. The resulting profile is plotted in Figure 5 (I_1, thick dashed line). We then repeat this synthesis but now including a

vertical magnetic field, $\gamma = 0^\circ$, with a strength of 1000 Gauss. The resulting profile is plotted in Figure 1 (I_2, thick solid line).

Next we perform a similar synthesis, where: a) we set the macroturbulent velocity to zero; b) we include a vertical field of 1000 Gauss and, c) we use a net line-of-sight velocity that changes from -4 km s^{-1} to 4 km s^{-1}. Each of the emerging profiles is indicated by one of the thin dashed lines in Fig. 1 (labeled as I_k). With this we try to simulate the effect of having different structures affected by convective velocity fields. We then add all those profiles using a weighting function with a Gaussian shape in order to mimic the macroturbulence. The resulting profile is indicated in Fig. 1 as I_3 (squares).

$$I_3 = \sum w_k I_k \tag{8}$$

$$w_k = \frac{v_{\rm mac}}{2}\sqrt{\frac{\pi}{\log 2}} e^{-4\log 2 \frac{v^2_{\rm los,k}}{v^2_{\rm mac}}} \tag{9}$$

where the FWHM of the Gaussian weighting function is equivalent to a macroturbulent velocity of 2 km s^{-1}. As it can be seen, $I_3 = I_2$. Therefore, the broadening due to convective motions does not hide the broadening produced by magnetic fields. Our simulations do not consider that this magnetic field is probably different in granules (upflows) and intergranules (downflows). We also use the same temperature stratification in all cases. Considering a more realistic case (using results from 3D MHD simulations) might yield slightly different results, but the same basic idea will apply also in that case. In this example we have used a relatively strong magnetic field (1000 Gauss) to facilitate a visual comparisons in Fig. 5, but it is worth mentioning that repeating the experiment with smaller fields leads to the same result.

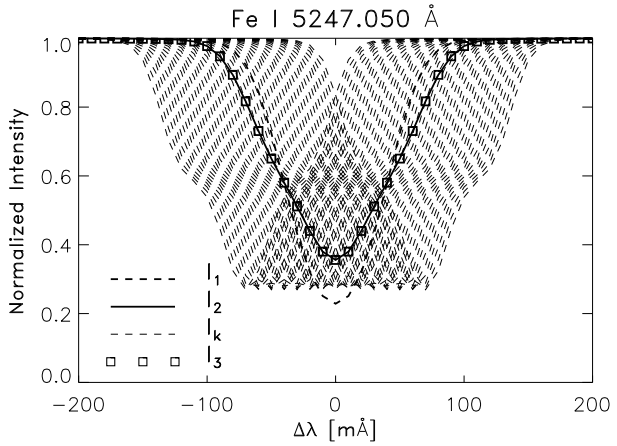

FIG. 5.— Simulated intensity profiles of Fe I 5257.050 Å. Thick dashed line, I_1 was obtained using a macroturbulent velocity of $v_{\rm mac} = 2$ km s^{-1}. In addition to this, we include a magnetic field with: $B = 1000$ Gauss and $\gamma = 0^\circ$, thus obtaining I_2 (thick solid). Individual thin dashed lines, I_k, were obtained with $v_{\rm mac} = 0$, $B = 1000$ Gauss and $\gamma = 0^\circ$ and a varying $v_{\rm los}$ from -4 km s^{-1} to 4 km s^{-1} to simulate a convective velocity field. All I_k are added up into I_4 according to Eq. 8 and 9.

To provide further support to our argument we have recalculated the effects of the magnetic fields in the abundance (as done in section 3) but using a smaller macroturbulence: $v_{\rm mac} = 1$ km s^{-1}. The resulting plots are identical to those in Fig. 2. This result might seem at odds with Eq. 7, since the new macroturbulent velocity changes the values of $\Delta\lambda$ and I_0. However, if we repeat the calculation of the calibration curves in Fig. 4 no differences are observed in $\Delta \log \epsilon$ as compared to the case with $v_{\rm mac} = 2$ km s^{-1}. In order for this to happen, the only possibility is that the horizontal axis changes. This results in a different calibration constant $\mathcal{A}(\gamma)$ but equal errors in the abundance.

6. CONCLUSIONS

Ignoring the broadening caused by the magnetic field when fitting the intensity profiles of spectral lines, may lead to an erroneous determination of atomic abundances in the Sun and other magnetically active stars. Although there have been previous works where the magnetic field has been considered (Kochukhov et al. 2004; Socas-Navarro & Norton 2007), to our knowledge this is the first systematic study aiming at quantifying the role of the magnetic field. Our results indicate that Fe I lines are more affected than lines from elements like Si I, C I or O I. We have shown that vertical magnetic fields lead to an underestimation of the real abundance, while horizontal fields tend to overestimate it. In a more real situation, where the spectral lines would receive contributions from magnetic fields with different inclinations, these two effect are likely to cancel each other, making the contribution of the magnetic field almost negligible with the exemption of perhaps Fe I. It is important to mention that the degeneracy between magnetic fields and abundances occurs only for small fields, since for very large magnetic fields, the spectral line is fully split in its different Zeemann components (see for example Nesvacil et al. 2004). We have also developed a phenomenological model that can used to determine if a particular spectral line is suitable for abundances studies that do not consider the effect of the magnetic field.

Our analysis 1D LTE analysis neglects the effect of having variations in temperature stratifications and/or convective velocities fields. Therefore, our results apply only if all those others possible sources of errors can be eliminated. If that was not the case, the error introduced by the magnetic field would be of second importance. This situation is highlighted by the work of Socas-Navarro & Norton (2007), who in spite of consistently considering the magnetic field, obtained strong discrepancies between the inferred abundances in quiet solar regions (e.g.: granulation) and magnetic regions (e.g.: pores). The source of those discrepancies is therefore to be ascribed to small (< 100 K) errors in the temperature stratification.

It would be ideal to repeat this work using realistic 3D MHD simulations (using several initial magnetic fluxes) in order to model more realistically the different temperatures, velocities, field strength and inclinations present in solar and stellar photospheres. However, our work does provide a first hint that magnetic fields are an unlike source of large errors in abundance determinations, unless a very particular spectral line or a very particular magnetic configuration is present.

I wish to thank Eberhard Wiehr for bringing up the issue, during a talk I gave at the University of Göttingen

in 2003, of using only spectral lines with zero Landé factor in abundance determinations. That warning led to consider the effects of the magnetic field whenever those were not available. Thanks also to Carlos Allende Prieto and an anonymous referee for important suggestions and comments.

REFERENCES

Allende Prieto, C., Asplund, M., López García, R.J. & Lambert, D. 2002, ApJ, 567, 544
Anstee, S.D. & O'Mara, B.J. 1995, MNRAS, 276, 859
Asplund, M., Nordlund, A., Trampedach, R. & Stein, R.F. 2000, A&A, 359, 743
Asplund, M. 2001, A&A, 2000, 359, 755
Asplund, M., Grevesse, N., Sauval, A.J., Allende Prieto, C. & Kiselman, D. 2004, A&A, 423, 1109
Asplund, M., Grevesse, N., Sauval, A.J., Allende Prieto, C. & Blomme, R. 2005a, A&A, 431, 693
Asplund, M., Grevesse, N., Sauval, A.J. 2005b, in Cosmic Abundances as Records of Stellar Evolution and Nucleosynthesis in honor of David Lambert, ASP Conference Series, 336, 25. Eds: Thomas G. Barnes III and Frank N. Bash.
Barklem, P.S. & O'Mara, B.J. 1997, MNRAS, 290, 102
Barklem, P.S., O'Mara, B.J. & Ross, J.E. 1998, MNRAS, 296, 1057
Barklem, P.S., Piskunov, N.E. & O'Mara, B.J. 2000, A&AS, 142, 467
Brault, J. & Neckel, H. 1987, Spectral atlas of the solar absolute disk-averaged and disk center intensity from 3290 Å to 12510 Å available at ftp.hs.uni-hamburg.de/pub/outgoing/FTS-atlas
Cabrera Solana, D., Bellot Rubio, L.R. & del Toro Iniesta, J.C. 2005, A&A, 439, 687
Castro, M., Vauclair, S. & Richard, O. 2007, A&A, 463, 755
Christlieb, N., Bessell, M. S., Beers, T. C., Gustafsson, B., Korn, A., Barklem, P. S., Karlsson, T., Mizuno-Wiedner, M. & Rossi, S. 2002, Nature, 419, 904
Garz, T., Holweger, H., Kock, M., Richter, J. 1969, A&A, 2, 446
Gingerich, O., Noyes, R.W., Kalkofen, W. & Cuny, Y. 1971, Sol. Phys., 18, 347
Grevesse, N. 1968, Sol. Phys., 5, 159
Kochukhov, O., Bagnulo, S., Wade, G. A., Sangalli, L., Piskunov, N., Landstreet, J. D., Petit, P., Sigut, T. A. A. 2004, A&A, 414, 613
Ichimoto, K. & Solar-B Team 2005, Journal of Korean Astronomical Society, 38, 307
Lambert, D.L. 1968, MNRAS, 138, 143
Lambert, D.L. & Warner, B. 1968, MNRAS, 138, 181
Landi Degl'Innocenti, E. 1976, A&AS, 25, 379
Lites, B.W., Elmore, D.F. & Streander, K.V. 2001, ASP Conf. Ser., 236, 33
Manso Sainz, R., Landi Degl'Innocenti, E. & Trujillo Bueno, J. 2004, ApJ, 614, L89
Neckel, H. 1999, Sol. Phys., 184, 421
Nesvacil, N., Hubrig, S. & Jehin, E. 2004, A&A, 422, 225
Ruiz Cobo, B. & del Toro Iniesta, J.C. 1992, ApJ, 398, 375
Socas-Navarro, H. & Norton, A.A. 2007, ApJ, 660, 153
Stein, B. & Nordlund, Å 2006, ApJ, 642, 1246
del Toro Iniesta, J.C. 2003, *Introduction to Spectropolarimetry*, Cambridge University Press, ISBN 0-521-81827-3
Trujillo Bueno, J., Shchukina, N. & Asensio Ramos, A. 2004, Nature, 430, 326
Vögler, A., Sheylag, S., Schüssler, M., Cattaneo, F., Emonet, T. & Linde, T. 2005, A&A, 429. 335
Wittmann, A. 1974, Sol. Phys., 35, 11

TABLE 1

SUMMARY OF EMPLOYED SPECTRAL LINES; TEMPERATURE PARAMETER α AND CROSS SECTION FOR COLLISIONS WITH NEUTRAL HYDROGEN (IN UNITS OF BOHR'S RADIUS a_0) FROM ABO THEORY (BARKLEM ET AL. 2000); LANDÉ FACTOR G_{eff} IS CALCULATED UNDER LS APPROXIMATION FROM THE ELECTRONIC CONFIGURATIONS OF THE UPPER AND LOWER LEVELS.

Atom	λ_0 [Å]	χ_l [eV]	$\log(gf)$	α	σ/a_0^2	g_{eff}	I_0	$\Delta\lambda$ [mÅ]	Lower Level	Upper Level
Fe I	4389.245	0.052	−4.583	0.249	217	1.50	0.338	52.30	5D3	7F2
Fe I	5247.050	0.087	−4.946	0.253	206	2.00	0.464	59.36	5D2	7D3
Fe I	5250.209	0.121	−4.938	0.253	207	3.00	0.471	59.21	5D0	7D1
Fe I	5412.798	4.434	−1.761	0.280	971	0.97	0.845	60.04	3G4	5H4
Fe I	5525.544	4.230	−1.084	0.238	748	1.50	0.559	66.65	5D0	5D1
Fe I	5701.544	2.559	−2.216	0.237	361	1.12	0.439	70.38	3F4	3D3
Fe I	5784.658	3.396	−2.530	0.244	796	1.87	0.781	64.04	5F3	5D4
Fe I	5956.694	0.859	−4.605	0.252	227	0.70	0.621	64.91	5F5	7P4
Fe I	6082.710	2.223	−3.573	0.271	306	2.00	0.745	65.48	5P1	3P1
Fe I	6136.994	2.198	−2.950	0.265	280	2.00	0.545	70.27	5P2	5D1
Fe I	6151.618	2.176	−3.299	0.263	277	1.83	0.639	67.74	5P3	5D2
Fe I	6173.335	2.223	−2.880	0.266	281	2.50	0.535	71.16	5P1	5D0
Fe I	6200.313	2.608	−2.437	0.235	350	1.50	0.522	73.08	3F2	3F3
Fe I	6219.280	2.198	−2.433	0.264	278	1.60	0.436	77.74	5P2	5D2
Fe I	6240.646	2.223	−3.230	0.272	301	1.00	0.634	68.97	5P1	3P2
Fe I	6265.133	2.176	−2.550	0.261	274	1.58	0.456	76.98	5P3	5D3
Fe I	6271.278	3.332	−2.703	0.247	720	1.50	0.821	69.31	5F5	7D5
Fe I	6280.618	0.859	−4.387	0.253	223	1.45	0.565	70.22	5F5	7F5
Fe I	6297.793	2.223	−2.740	0.264	278	1.00	0.507	74.31	5P1	5D2
Fe I	6322.685	2.588	−2.426	0.238	345	1.50	0.520	75.02	3F3	3F4
Fe I	6481.870	2.279	−2.984	0.243	308	1.50	0.587	73.46	3P2	5D2
Fe I	6498.939	0.958	−4.699	0.253	226	1.37	0.698	69.81	5F3	7F3
Fe I	6581.210	1.485	−4.680	0.245	254	1.30	0.859	68.69	3F4	5F4
Fe I	6593.870	2.433	−2.422	0.247	321	1.15	0.496	79.91	3H5	5G5
Fe I	6609.110	2.559	−2.692	0.245	335	1.15	0.589	75.30	3F4	3G4
Fe I	6750.152	2.424	−2.621	0.241	335	1.50	0.542	79.42	3P1	3P1
Fe I	6945.205	2.424	−2.482	0.243	331	1.50	0.519	84.01	3P1	3P2
Fe I	6978.851	2.484	−2.500	0.241	337	1.50	0.536	83.43	3P0	3P1
Fe I	7723.208	2.279	−3.617	0.242	304	1.17	0.794	82.56	3P2	3D3
Si I	5645.613	4.93	−2.04	0.223	1791	1.75	0.748	74.38	3P1	3S1
Si I	5665.555	4.92	−1.94	0.222	1772	0.00	0.708	75.76	3P0	3P0
Si I	5684.484	4.95	−1.55	0.221	1797	1.25	0.570	82.41	3P2	3S1
Si I	5690.425	4.93	−1.77	0.222	1772	1.50	0.646	78.42	3P1	3P1
Si I	5701.104	4.93	−1.95	0.222	1767	1.50	0.716	76.06	3P1	3P0
Si I	5708.400	4.95	−1.37	0.222	1787	1.50	0.509	87.37	3P2	3P2
Si I	5772.146	5.08	−1.65	0.207	2036	1.00	0.660	81.16	1P1	1S0
Si I	5780.384	4.92	−2.25	0.228	1691	0.50	0.819	74.28	3P0	3D1
Si I	5793.073	4.93	−1.96	0.228	1703	1.00	0.723	77.01	3P1	3D2
Si I	5797.856	4.95	−1.95	0.223	1755	1.16	0.727	77.27	3P2	3D3
Si I	5948.541	5.08	−1.13	0.222	1845	1.00	0.491	96.52	1P1	1D2
Si I	7680.266	5.86	−0.59	0.495	2106	1.00	0.631	126.0	1P1	1D2
Si I	7918.384	5.95	−0.51	0.232	2933	0.75	0.643	141.8	3D1	3F2
Si I	7932.348	5.96	−0.37	0.235	2985	1.00	0.610	150.3	3D2	3F3
Si I	7970.307	5.96	−1.37	0.232	2927	0.92	0.883	117.0	3D2	3F2
C I	7111.469	8.640	−1.074	0.313	1842	0.75	0.941	121.1	3D1	3F2
C I	7113.179	8.647	−0.762	0.314	1857	1.12	0.903	125.4	3D3	3F4
C I	9603.036	7.480	−0.895	0.236	561	2.00	0.752	175.4	3P0	3S1
C I	10753.976	7.488	−1.598	0.238	532	2.00	0.875	174.5	3P2	3D1
C I	11777.546	8.643	−0.490	0.271	746	0.92	0.854	214.1	3D2	3F2
C I	12549.493	8.847	−0.545	0.293	863	1.50	0.880	228.0	3P0	3P1
C I	12562.124	8.848	−0.504	0.293	863	1.50	0.874	230.6	3P1	3P0
C I	12569.042	8.848	−0.586	0.293	863	1.50	0.885	226.3	3P1	3P1
C I	12581.585	8.848	−0.509	0.293	862	1.50	0.874	230.9	3P1	3P2
O I	6158.176	10.74	−0.30	0.322	1915	1.58	0.976	98.30	5P3	5D3
O I	7771.944	9.15	0.37	0.234	452	1.33	0.734	134.04	5S2	5P3
O I	7774.166	9.15	0.22	0.234	452	1.92	0.761	129.76	5S2	5P2
O I	7775.388	9.15	0.00	0.234	452	1.75	0.800	124.15	5S2	5P1